PSF far wings and "red halo" in the photometry of galaxies. One more source of errors

R. Michard

A&A 384, 763–771 (2002)
DOI: 10.1051/0004-6361:20011813

Astronomy & Astrophysics

PSF far wings and "red halo" in the photometry of galaxies

One more source of errors⋆

R. Michard⋆⋆

Observatoire de Paris, LERMA, 77 Av. Denfert-Rochereau, 75015, Paris, France

Received 29 August 2001 / Accepted 28 November 2001

Abstract. PSF far wings have been measured in *UBVRi* at the 120 cm Newtonian telescope of Observatoire de Haute Provence, during 3 observing runs in 2000-1. The choice of appropriate star fields allowed us to extend the measurements up to a radius of nearly 3 arcmin, and down to a level of about 0.5×10^{-6} of the central peak. It was found that these wings, farther than a radius of 15 arcsec, do not change with atmospheric seeing, but are dependent on the spectral passband and the time elapsed since the coating of the mirrors. The most prominent spectral effect is the "red halo" occurring with thinned CCDs, but PSF wings in U, B, and R may also stand above the V light wings. All PSF wings were greatly reinforced after 10 months of mirror ageing. The consequences of the far PSF wings for galaxy surface photometry and colorimetry have been studied by convolution of models with the measured PSF. Gray models of E-type objects acquire spurious colour gradients, large enough in $V - i$ to reverse the classically measured ones, and sufficient in $U - B$ or $U - V$ to significantly bias the results. The colours along the major and minor axis are unequally affected for flattened objects. Experiments with a model of the lenticular NGC 3115 show that spurious disk colours may also be introduced. It has been verified that the effects of the "red halo" on $V - i$ colour gradients may be corrected by convolving the frame i with the V PSF and conversely, before measuring the colour distribution. The same is true for the lesser effects in other colours. These "corrections" are made at the expense of resolution and cause further uncertainties in the results.

Key words. galaxies: elliptical and lenticulars, cD – galaxies: photometry

1. Introduction

When using recent OHP frames to complete the previous discussion of colour gradients in ellipticals in Michard (2000), it was noticed that the haloes around overexposed stars were much more intense in the i band than in the other colours: we learned that this unfortunate property of thinned CCDs had been termed "red halo" by the experts. It was then tried to measure the outer wings of PSF from the available frames, and also to ascertain the effects of the red halo upon colour gradients. These were found to be quite large, since the "classical" negative colour gradients in $V - i$ measured by Bender & Möllenhof (1987) or Goudfrooij et al. (1994), turned positive (strongly so in some cases), but they could not however be well predicted, due to an insufficient radial range in the PSF measurements. Attempts to correct the gradients led to unreliable results, for the same reason.

The red halo of thinned CCDs is of course not the only cause of the *extended wings* of PSF. The question has been considered very early in galaxy photometry (de Vaucouleurs 1948; King 1971). Capaccioli & de Vaucouleurs (1983) (CdV83) measured an "aureole" around bright stars, surrounding the central "image" dominated by atmospheric "seeing". This was attributed to "scattering by fine particles in suspension in the atmosphere or deposited on the mirrors". They showed that the aureole could affect the results of galaxy photometry in the external parts of such extended objects. Light scattered by the mirrors and by the atmosphere was also a worry to solar physicists, in the epoch of ground based coronography, or in sunspot photometry. Michard (1953), measured the scattered light at 1 arcmin from the solar limb, and found its colour to be very blue, although less than in pure Rayleigh scattering. A significant increase within 3 months after coating of the 4 mirrors system was noted.

A more continuous effort was devoted to the study of the *central core* of the PSF, which determines the angular resolution attained. Its effects upon the geometry

⋆ Based on observations collected at the Observatoire de Haute-Provence.

⋆⋆ e-mail: Raymond.Michard@obspm.fr

and photometry of celestial sources are more obvious and spectacular than the discreet ones of the far wings. In the domain of galaxy photometry, we may quote significant contributions by Schweizer (1979, 1981), Franx et al. (1989), Peletier et al. (1990). More recently the advent of the HST, both in its initial and "refurbished" states, lead to many studies of PSF modelization and their use to recover improved data by deconvolution (see Mo & Hanisch 1993 and other contributions at the same meeting). Besides the HST applications, such work as Hasan & Burrows (1995) are precious because they review the physics of image degradation from various sources, other than atmospheric seeing (and the red halo!).

In the present work we use new OHP observations of selected stars to measure accurately the *outer wings* of the PSF in *UBVRi*, to study their variation with colour (including the "red halo" phenomenon), and their eventual changes with time, i.e. with the age of the coating of the telescope mirrors. On the other hand we study the effects of PSF far wings on the results of galaxy photometry, and especially the colour distribution in these objects, using model calculations. Differences in the PSF far wings of the two pass bands involved in a colour, may indeed produce significant errors in local colours. While an error of 0.1 mag in the surface brightness of a galaxy near $\mu_B = 25$ will perhaps not be considered important, such an error in colour may change enormously a colour gradient.

Finally a technique to correct errors in galaxy colour distributions due to PSF differences is investigated. It consists of convolving frame A with the PSF of frame B and conversely, before measuring the colour $A - B$. Some requirements and precautions in the use of this procedure with very extended PSF are noted. The technique has been extensively used in a survey of the *UBVRi* colour distributions of 40 galaxies, mostly elliptical (see Idiart et al. 2002). Its full success has been proven by the study of internal and external errors.

2. Measurements of PSF wings

2.1. Observations and data reduction

2.1.1. Observations

The observations were obtained during a new survey of colour distributions in E-type galaxies started in 2000 by T. Idiart, R. Michard, J. de F. Pacheco and P. Prugniel. We used the 120 cm Newtonian telescope of the Observatoire de Haute-Provence, in three runs: April 1/11 2000, May 29/June 5 2000 and January 18/29 2001, quoted below as *run 1, 2 and 3*. A CCD target Tek1024 is mounted in the camera, giving a field of view of 11.6×11.6 arcmin for a pixel size of 24 microns or 0.68 arcsec. At the OHP, the *FWHM* of stellar images is usually in the 2–3 arcsec range, with values at 4 or more during periods of northern wind (mistral). The filters used in *UBVR* approximate the Cousins's system, while the *i* is after Gunn.

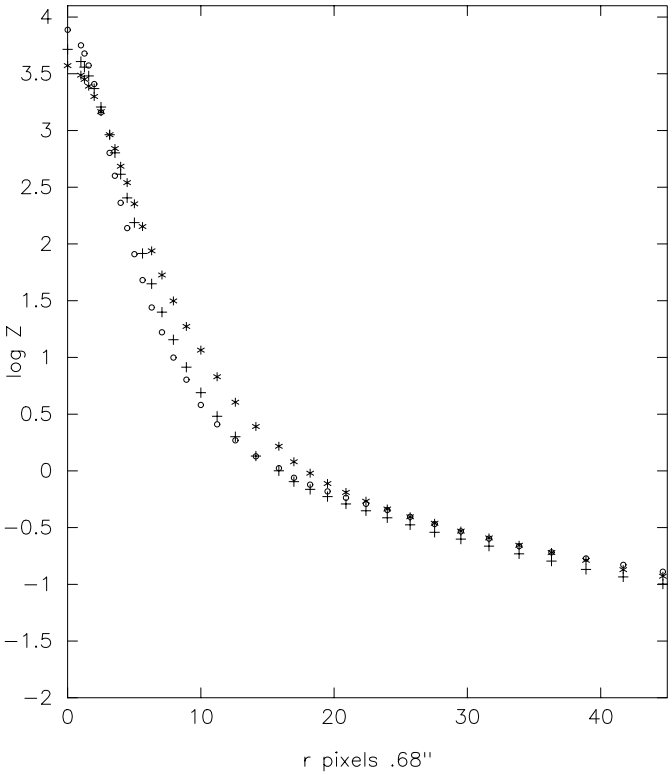

Fig. 1. A set of three V PSF measured in *run 1* in various seeing conditions. The various curves merge near $r = 20$ pixels or about 14 arcsec.

Stellar fields deemed suitable for measuring the outermost PSF wings were selected beforehand for these observations from an inspection of prints of the PSS, far from the Galaxy: they had to contain one bright star, *badly saturated to allow the detection of PSF wings far from the center*, one or several unsaturated stars, bright enough however for the derivation of a good central profile, and one or two stars of intermediate exposures, needed to bridge the gap between the central core and outermost wings. The method of selection garantees a rather "clean" background, the presence of a large galaxy or of any nearby bright object being of course avoided.

2.1.2. Measurement of PSF

The derivation of one PSF involved a routine with the following steps:

- The sky background throughout the field was mapped and substracted;
- For each selected PSF star, normally 4 in a given field, the average intensity was measured on concentric circles, excluding the central "bad" columns of saturated images;
- The profiles for each star were then combined using the radial range where they are proportional, outside the ranges affected either by saturation or by large background uncertainties. The resulting profile was then

Table 1. Values of the surface brightness of measured mean PSF at selected radii, in a logarithmic scale. These can be intercompared because they are normalized within a constant radius of $r = 159.1''$, where the integrated intensity is assumed to be 10^5. The central intensity varies because of different seeing in the observations used. For runs 1 and 3, the quoted standard errors are derived from the dispersion of 4 to 7 measures. For run 2, only one measure was available, and the quoted error is estimated from the dispersions in the other runs. No B PSF is available for run 1.

run No.	r''	U	B	V	R	i
run 1	0.0	$3.59 \pm .04$	–	$3.60 \pm .10$	$3.61 \pm .08$	$3.69 \pm .10$
run 1	21.5	$-0.49 \pm .01$	–	$-0.63 \pm .01$	$-0.48 \pm .01$	$-0.15 \pm .01$
run 1	42.9	$-1.05 \pm .02$	–	$-1.24 \pm .01$	$-1.08 \pm .01$	$-0.69 \pm .01$
run 1	85.6	$-1.76 \pm .02$	–	$-1.88 \pm .03$	$-1.76 \pm .02$	$-1.45 \pm .02$
run 1	120.9	$-2.24 \pm .05$	–	$-2.27 \pm .06$	$-2.19 \pm .03$	$-1.95 \pm .03$
run 1	170.8	$-2.77 \pm .08$	–	$-2.73 \pm .07$	$-2.64 \pm .04$	$-2.48 \pm .03$
run 2	0.0	$3.59 \pm .00$	$3.63 \pm .00$	$3.62 \pm .00$	$3.70 \pm .00$	$3.67 \pm .00$
run 2	21.5	$-0.40 \pm .02$	$-0.51 \pm .02$	$-0.57 \pm .02$	$-0.51 \pm .02$	$-0.18 \pm .01$
run 2	42.9	$-1.03 \pm .04$	$-1.16 \pm .04$	$-1.22 \pm .04$	$-1.13 \pm .04$	$-0.74 \pm .02$
run 2	85.6	$-1.78 \pm .12$	$-1.79 \pm .12$	$-1.88 \pm .08$	$-1.83 \pm .08$	$-1.55 \pm .04$
run 2	120.9	–	$-2.16 \pm .16$	$-2.22 \pm .10$	$-2.24 \pm .10$	$-2.05 \pm .06$
run 2	170.8	–	$-2.41 \pm .20$	$-2.44 \pm .15$	$-2.48 \pm .15$	$-2.33 \pm .08$
run 3	0.0	$3.58 \pm .03$	$3.58 \pm .03$	$3.56 \pm .06$	$3.71 \pm .06$	$3.59 \pm .04$
run 3	21.5	$-0.05 \pm .01$	$-0.09 \pm .01$	$-0.20 \pm .02$	$-0.24 \pm .02$	$-0.08 \pm .01$
run 3	42.9	$-0.72 \pm .02$	$-0.79 \pm .02$	$-0.84 \pm .02$	$-0.82 \pm .01$	$-0.59 \pm .01$
run 3	85.6	$-1.38 \pm .06$	$-1.48 \pm .07$	$-1.59 \pm .03$	$-1.57 \pm .03$	$-1.33 \pm .02$
run 3	120.9	$-1.80 \pm .09$	$-1.85 \pm .10$	$-1.97 \pm .06$	$-2.00 \pm .06$	$-1.80 \pm .04$
run 3	170.8	$-2.24 \pm .14$	$-2.27 \pm .13$	$-2.33 \pm .06$	$-2.33 \pm .07$	$-2.25 \pm .04$

normalized using a large radial range, within a radius of near 160 arcsec, to obtain one PSF;

Several PSF in each colour were measured, 4 to 7 in *run 1*, with two star fields used, one in *run 2*, and 4 to 6 in *run 3* for three star fields. This allowed us to check the stability of the PSF far wings, and to estimate probable errors in their derivation. Since it was known from previous experience that the B and V PSF profiles were very similar, it was at first thought unnecessary to measure both. For the second and third runs, however, the B profiles were also measured. Finally the various profiles obtained for each observing run were averaged to obtain the mean PSF for the epoch and colour.

Table 1 gives selected measurements of mean PSF wings: for *run 1* and *run 3* there are sufficient data for a calculation of standard errors. For *run 2* the errors are taken to be the dispersion of the previous series, and are less reliable. *It should be emphasized that the PSF wings are generally measured up to a radius of 180 arcsec and down to a level below* 10^{-6} *of their peak brightness.*

2.1.3. Discussion of errors

Noise-induced errors are negligible here, because of the huge numbers of pixels involved in the derivation of a PSF profile (outside the core!), and also the large number of profiles used to build a mean PSF. More significant sources of errors are:

a) from the fit of several radial ranges of stellar profiles to build up a single PSF. We are unable to present an independant estimate of the corresponding errors;

b) errors in the evaluation of the sky background. These however enter only at the largest measured radii, farther than $r = 2'$. The average error in background has been estimated to be 0.09%: this corresponds to roughly -3.3 in the scale of Table 1 and in V light. Numerical simulations have ben performed to get more insight into errors induced by imperfect sky background estimates: overestimating the background leads to a rather abrupt cutoff of the PSF wings, i.e. a rather obvious signature; underestimating it, flattens the outer wing gradient in a less evident manner. Such effects are below easy detection in the retained profiles. As regards this class of errors, the situation is more favourable in i due to the brighter wings, less favourable in U where residual background fluctuations are larger.

Error estimates in Table 1 are obtained by a straightforward method: since $n = 4$ to 7 PSF profiles are available for each PSF, we may calculate the dispersion of measurements, hence the probable error of their mean. This takes into account all source of errors, notably a) and b) above.

Remark: It is not unlikely that the standard errors given in the table are underestimated. The statistics are quite limited, and individual measures possibly do not belong to a normal distribution. The variations in PSF

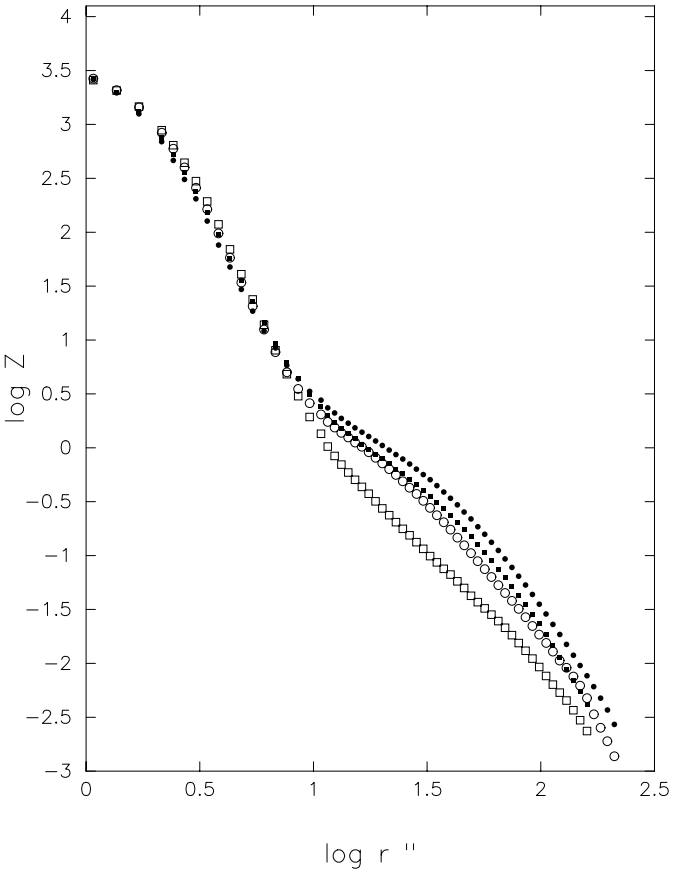

Fig. 2. Radial profiles of the mean PSF in V and i for two runs. Abscissae: $\log r''$. Ordinates: PSF brightness in logarithmic scale, with open squares for V in run 1, open circles for V in run 3, the same filled symbols for i in the two runs. Errors bars are generally smaller than data points: see Table 2 for estimated probable errors. Due to the red halo effect, the i PSF are well above the V ones. In the 10 months between the runs, the V PSF far wings strongly brightened, less so for the i PSF, possibly due to ageing of the mirror coating. Both the colour and time effects start below $r < 10''$ and are maximum in a range of quite reliable measurements.

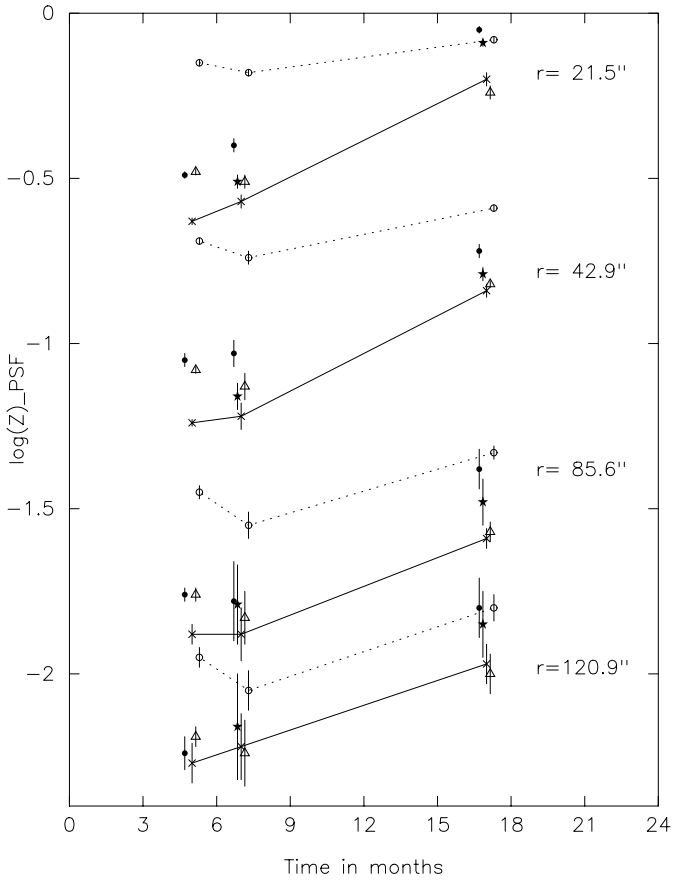

Fig. 3. Time variations of logarithmic intensities of PSF wings at selected radii from data in Table 1. Abscissae: time in months elapsed since mirror coating. Ordinates: residual brightnesses taken from Table 1, with dots for U, stars for B, oblique crosses for V, triangles for R and circles for i. For better clarity, the data points for V and i are joined by a line, dotted in the later case. Note that the largest time changes occur in the radial range of negligible errors.

measured in different star fields are indeed greater than found for the same field in different nights.

2.1.4. Comparison with a classical measurement

Our V PSF have been compared with the profile of CdV83 (their Table 4), who derive the far wings from photoelectric drift curves of very bright stars, i.e. γCMa and αCMa. They express surface brightnesses in an absolute unit, i.e. B magnitudes per arcsec squ. in the image of a star with $B = 0$ outside the atmosphere. Our data were tentatively converted to this unit with a correction taking into account the different radial ranges used in the respective normalizations. The agreement is rather poor, which is not surprising in view of the large uncertainties in this kind of measurements. In a large range, drift curve data of CdV83 lies between our results for *run 1 and 3*. Our far wing gradients are however steeper. Also note that the asymptotic value of the PSF is zero in our case, while in CdV83 it is finite, and equal to the estimated Rayleigh scattering at very large elongations.

2.2. Review of PSF properties measured

The empirical results from the present series of PSF measurements will now be reviewed.

1. In the inner radial range, and up to a few arcsec in r, the form of the PSF are determined by atmospheric seeing. This is especially true for a site of admittedly rather poor seeing. Around $r = 15$ arcsec, the seeing effects disappear and the PSF are controlled by instrumental and atmospheric scattering. At this radial distance, the PSF in a given pass band and a given run tend to merge, as shown in Fig. 1;
2. In the range outwards of $r = 15$, *the i PSF is well above the V PSF*. This excess is already apparent near $r = 6''$, or about twice the *FWHM* of the PSF. The excess reaches a factor of 3 or more around $r = 40$

Table 2. Comparison of PSF far wings with the one in V light. The indices ΔUV, etc. are defined in the text. Relative intensities and errors are extracted from Table 1.

Date	ΔUV	ΔBV	ΔRV	ΔIV
run 1	$0.15 \pm .04$	–	$0.14 \pm .04$	$0.45 \pm .03$
run 2	$0.15 \pm .11$	$0.07 \pm .11$	$0.14 \pm .09$	$0.41 \pm .07$
run 3	$0.16 \pm .07$	$0.08 \pm .07$	$0.02 \pm .05$	$0.26 \pm .03$

to 60″, and tends to decrease farther out (see data for *run 1* in Table 1). This is the "red halo" effect of thinned CCDs. This effect is displayed in Fig. 2 for the mean data of *run 1* and *run 3* respectively. Both sets of data show the i PSF well above the V one in a large radial range. With the *run 1* data the i excess is 5 to 25 times larger than the combined errors quoted in Table 1. It is smaller for *run 3* but still quite significant;

3. The PSF far wings show *remarkable variations in time*, being brighter in all colours in *run 3* than in *run 1*, *run 2* being intermediate, within the accuracy of the data. These time variations are tentatively associated with the ageing of the telescope mirrors coating. These were recoated 5 months before *run 1*. In Fig. 3 the wing brightness of Table 1, is plotted against time in months: they increase strongly with time in UBV, but less in R and very little in the IR. We emphasize that the time variations in V wings are the strongest at the inner plotted radius, i.e. $r = 21.5''$, where errors of measurement are negligible.
4. Besides the "red halo" effect of the i band, there are small differences between the PSF far wings in $UBVR$, the V band being the faintest in all the runs. Taking as a measure of these differences an index $\Delta AV = \log i_A - \log i_V$, where $\log i_A$ and $\log i_V$ are the tabulated intensities in Table 1 for colours A and V respectively, averaged for the radii 42.9 and 85.6, we find the results of Table 2, with probable errors derived from those in Table 1.
   It appears that the differences between the U, B and V PSF remained constant, while the excess of the R PSF measured in April 2000 disappeared in the winter 2001 run, obviously because the V wings brightened much more than the R ones. Similarly the excess of the i PSF above the V one is greatly reduced in *run 3* as compared to *run 1*; in other words the red halo effect decreased with time at this telescope in 2000-1! These curious variations are independently confirmed by the statistics of E galaxies radial colour gradients in $V - R$ and $V - i$ obtained during the 3 runs, as discussed in Idiart et al. (2002).

The red halo effect, as expressed in the ΔIV indices of Table 2, is 6 times bigger than the calculated errors in *run 2* and 8–12 bigger in the other runs! On the other hand, the differences are smaller and the errors larger, for the PSF of other pairs of colours, so that the difference in B and V is probably not significant, while one might question the significance of the U excess.

3. Effects of PSF wings on galaxy surface brightness and colour measurements

We now present the results of the convolutions of galaxy models by the PSF measured here. The tabulated PSF profiles were used to produce synthetic PSF images, of 512×512 pixels. In some cases, a little extrapolation is needed to fill up the corners of the square: an exponential decrease is assumed, and fitted to the outer measured data points. The synthetic mean PSF in the various colours were brought to the same $FWHM$, by ad hoc deconvolutions with narrow Gaussians: in this way it can be assumed that the colour effects produced by the further convolution of models are essentially due to differences in the far wings of the PSF used.

Remark: We have tested the eventual influence of the unavoidable outer cut-off of PSF wings on the results of the convolutions. For this purpose we compared the results obtained with a set of V and i PSF of 801×801 pixels (involving some extrapolation!) and the same truncated at 501×501 and 301×301. It was found that the adopted format of 512×512 is adequate to avoid significant errors associated with the truncation.

3.1. Results for a model of NGC 4473

A model of NGC 4473 was built by merging a high-resolution CFHT image with a deep, wide field, OHP frame. Rather than combining the images themselves, we prefer to merge the numerical files containing the results of the isophotal analysis of the respective frames, performed according to Carter (1978). A synthetic model image is then built from the file of parameters resulting from this operation. The model retains the resolution of the CFHT frame ($FWHM$ 0.6″), with the proper values of the main geometrical parameters. Such a model is of course much less peaked at the center than the $r^{1/4}$ law, or than the HST measured profiles.

This model has been convolved with the mean PSF of *run 1* and *run 3*, and also for comparison with Gaussians of the same $FWHM$ as these measured PSF. In Fig. 4 the surface brightness distributions of the model after convolution by the PSF of *run 1* on the one hand, and by the Gaussian on the other, are compared. In the same figure, the same comparison is presented for the PSF of *run 3* and the corresponding Gaussian. The PSF wings have a significant effect on the magnitudes in both the central and outermost regions of the galaxy. These effects are minimal in the V band, the one having the faintest wings, and maximal in the i band due to the "red halo". Still in the V band, but also in the others, the wing effects are relatively small for the PSF of April 2000, but become quite large for the PSF of January 2001 with their much strengthened wings. Note that the attenuation due to the PSF wings is larger in the central galaxy regions than the excess light at the galaxy outskirts. In V light, the central attenuation induced by the wings is 0.14 mag with the PSF of *run 1*, but reaches 0.26 for the PSF of *run 3* (out

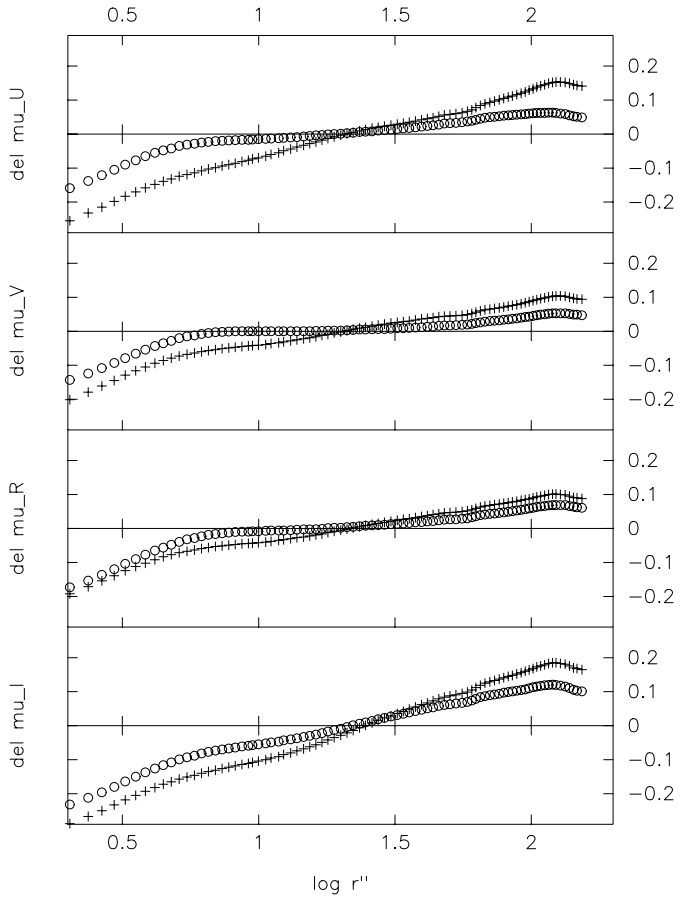

Fig. 4. Comparison between the surface brightness distributions of a model of NGC 4473 convolved by the measured PSF and by Gaussians of the same *FWHM*. Abscissae: logarithm of the isophotal radius. Ordinates: magnitude differences between the images convolved either with the real PSF or with the Gaussian. PSF of *run 1*: circles. PSF of *run 3*: crosses. Four pair of curves are shown for the passbands U, V, R and i.

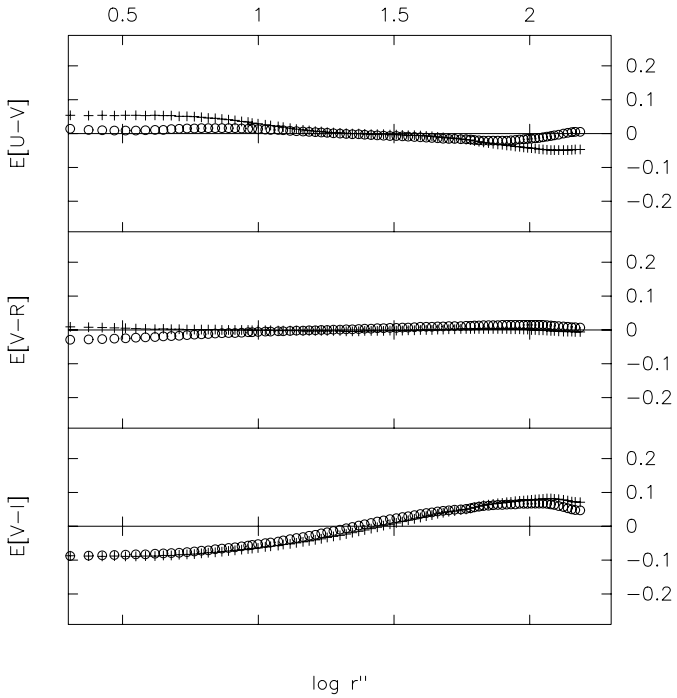

Fig. 5. Colour effects in $U-V$, $V-R$ and $V-i$ induced by PSF far wings for a model of NGC 4473. Abscissae: logarithm of the isophotal radius. Ordinates: Pseudo-colours induced by the convolutions. Circles: with the PSF of *run 1*. Crosses: with the PSF of *run 3*.

of a total attenuation of about 0.8 mag). Near $\mu_V = 25$ the brightening due to the V PSF wings varies from 0.1 to 0.2 mag.

The colour effects of the various PSF far wings are summarized in Fig. 5, showing the pseudo-colours induced by the convolution with measured PSF, both for the series of *run 1* and *run 3*. The colours $U-V$, $V-R$ and $V-i$ are considered. The $B-V$ effect is much smaller and considered negligible.

From Fig. 5, it appears that the measured colour gradients in $U-V$*, which amount to about* $d\log(U-V)/d\log r = -0.22$*, are still slightly lessened by the systematic differences in the corresponding PSF wings. The gradients* $\mathrm{d}\log(V-i)/\mathrm{d}\log r$ *with a mean of* -0.07*, are made strongly positive by the "red halo" effect. Finally the gradients* $\mathrm{d}\log(V-R)/\mathrm{d}\log r$*, with a mean of* -0.015*, are made slightly positive by the PSF of* run 1*, but are unchanged by those of* run 3.

3.2. Results for other models of E galaxies

The effects of the "red halo" on the colour distributions of other model galaxies have been considered. The models were derived in the same way as indicated above for the model of NGC 4473. The model for NGC 4550 however was obtained by partial deconvolution of an OHP V frame. This much elongated object is classified E7 by Sandage & Tammann (1981), but Michard & Marchal (1994) believe it to be an SA0.

In Fig. 6 we compare the pseudo-colours in $V-i$ induced by convolution with the measured PSF of *run 1* for models of NGC 4406 (a giant E3), NGC 4473, (an E5 of average size), NGC 4551 (a roundish minor object) and NGC 4550 (also a small galaxy but much flatter than its companion). The calculations *verify the expected result, i.e. that the effects of the PSF wings is larger for smaller objects and also larger for flatter objects of a given size*. In this case, light is transfered from the major to the minor axis of the image, with changes in the axis ratio and a strong variation in the respective colours at a given radius along the axis.

3.3. Results for a model of NGC 3115

This well-known nearly edge-on lenticular contains a bright thin disk embedded in a spheroidal halo. Analysis in terms of bulge+disk components have been published by Scorza & Bender (1995), and by Michard (1998). A gray model was obtained by merging a high resolution

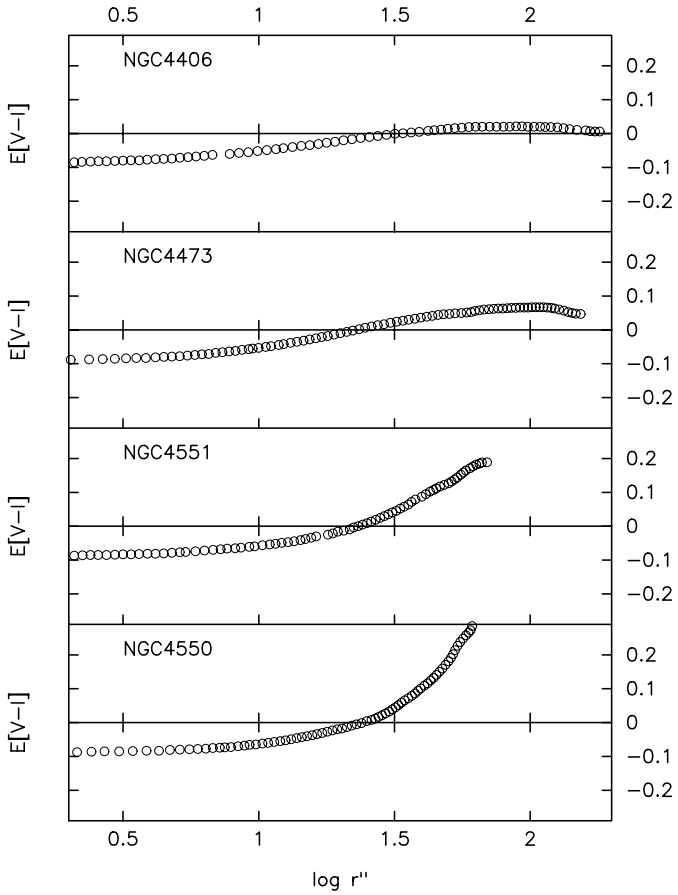

Fig. 6. Pseudo $V - i$ colours for models of several galaxies after convolution with the PSF of run 1. Completely spurious results are introduced by the "red halo" effect, especially for the smaller and flatter objects.

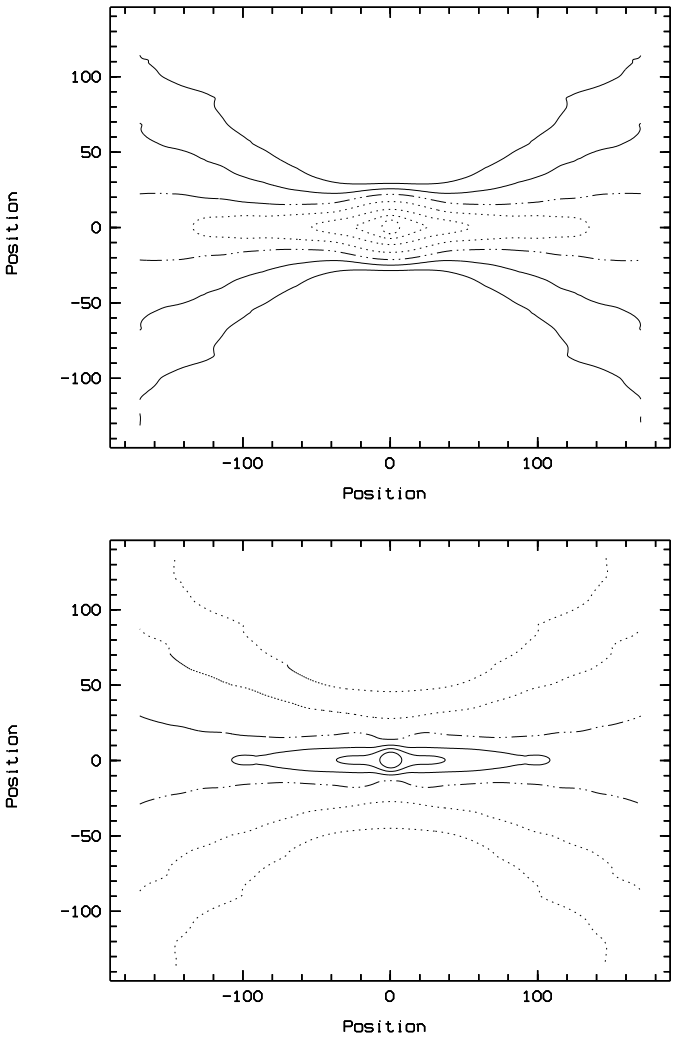

Fig. 7. Pseudo-colours induced by convolution of a model of NGC 3115, using the measured PSF of run 3. The positions are in arcsec. Upper frame: $V - i$ with isochromes at levels from 0.06 mag to −0.08 (center) in steps of 0.02. Blue colours are shown by dotted lines, red colours by full lines, the zero isochrome by a dash-dotted line. Note the blue disk and redder minor axis in the halo. Lower frame: $U - V$ with isochromes at levels from −0.03 mag to 0.045 (center) in steps of 0.015. Same convention as above for the sign of the colours. Note the red disk and bluer minor axis in the halo.

CFHT frame, with a deep, wide field, OHP image, and the effects of PSF wings on the structure and colours of this model were studied. As above, a set of *UBVRi* images have been obtained by convolution of the model synthetic image by the measured PSF, taken from *run 3* in this case. Geometrical parameters were compared, and pseudo-colours distributions induced by the PSF wings were measured and mapped.

As expected, the axis ratio, and also the Carter's cosine 4th harmonic, are affected by the PSF wings. For NGC 3115, the minimum axis ratio at a major axis $a =$ 100 arcsec is 0.36 for the V convolved frame, and increases to 0.38 for the i one. Colour effects are displayed in Fig. 7: it shows, in the form of isochromes, the pseudo-colours induced by the different PSF wings in $U - V$ and $V - i$. It appears that both a study of the disk colours and a comparison of the minor and major axis halo colours will be badly affected by the differences in the outer PSF wings. This occurs not only in $V - i$ because of the "red halo", but also in $U - V$, although the U wing excess is lower than the i one.

4. Correction of colours for the red halo effect

The errors in colour distribution resulting from different PSF in the two frames used may be corrected by convolving frame A with the PSF of frame B and conversely, before measuring the colour $A - B$. *It has been verified that this technique is adequate to correct for the effects of the "red halo" and of other colour differences in PSF wings.* Of course these "corrections" are made at the expense of resolution and add further uncertainties in the results. No comments are needed about the loss of resolution, but we may emphasize that errors in the PSF profiles lead to photometric errors in the convolved images. A new source of errors is introduced in the derivation of colour

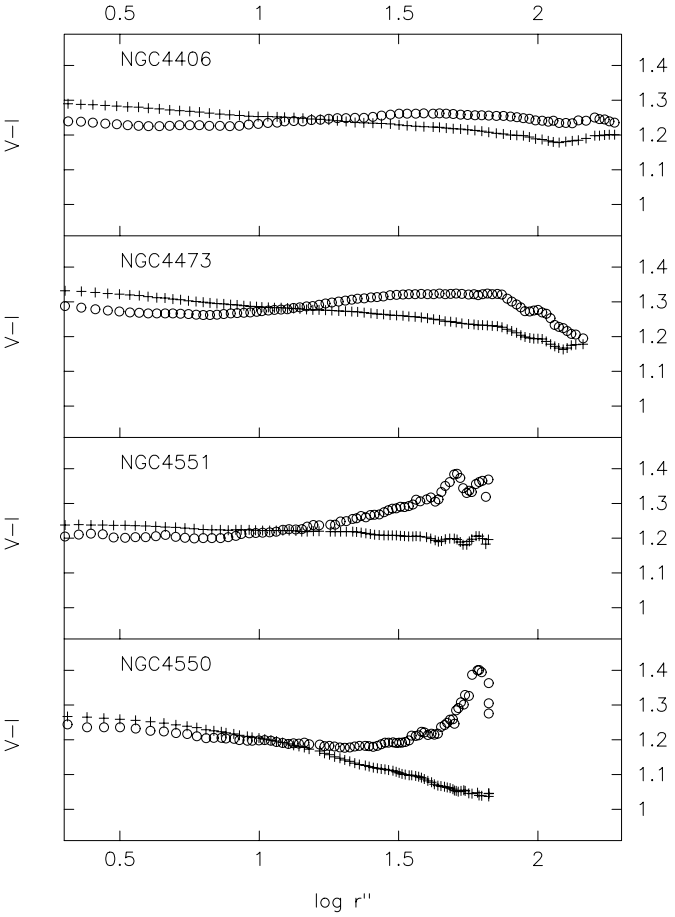

Fig. 8. Plots of the relation $V-i$ against $\log r$ are presented for "observed" frames (circles) and "corrected" by crossed convolutions (crosses). Abscissae: $\log r$ in arcsec. Ordinates: $V-i$ index in Cousins's system. Compare with Fig. 7 showing the effect of the PSF on models of the same objects.

distributions, notably the colour gradients in E-type objects, already plagued with various uncertainties.

A warning: the convolutions introduced here depress the central areas of the images. The V image, being convolved by the broader i PSF is more affected, and therefore the brightness and/or colour calibrations made before the crossed convolutions are no longer valid. While the colour gradient is corrected, its zero point becomes wrong. A correction of this effect is however easily found, for instance by repeating the comparison with aperture photometry of the convolved images.

Figure 8 presents a comparison of the $V-i$ against $\log r$ relations for 4 ellipticals before and after correction. The objects are the same as the PSF-convolved models of Fig. 6. The "observed" $V-i$ relations are similar to the corresponding models, except that the genuine negative colour gradients are superimposed on the strongly positive gradients resulting from the "red halo" effect. The classical negative gradients are restored in the "corrected" relations. Sky background errors may affect both the "observed" and "corrected" relations.

5. Discussion and conclusion

This study of the far wings of PSF in the Newtonian 120 cm telescope of the OHP leaves many questions unanswered and suggests that further work of the same kind might be useful.

The "red halo" of thinned CCDs is a fairly obvious effect, certainly well known to experts. It can be eliminated, or reduced, only at a very early stage in instrument design. Sirianni et al. (1998) found that the red halo could degrade very much the performance of the so-called Advanced Camera for Surveys, intended as an HST third generation instrument, and could obtain a solution from the SITe CCD maker. Lesser & Venkatranan (1998) propose a seemingly similar solution to avoid the loss of quantum efficiency in the near IR due to light transmission in the Si CCD layer, which is also responsible for the red halo. We are not certain, however, that observers were fully aware of possible errors from this effect in various work performed with common thinned CCDs, and involving $V-i$ comparisons.

For the study of colour gradients in E-type galaxies, the effect of the red halo was so obvious that we had to address the problem of its measurement and of its correction.

The more general problem of the existence of extended wings to the PSF, due to the instrument and atmosphere, has received seemingly little attention in recent years. In CdV83 the authors do not consider possible wavelength variations of the so-called "aureole", and neither possible time variations. According to our results however, both wavelength and time variations *do exist*, apart from the too obvious "red halo".

A variety of phenomena leading to image degradation, besides the atmospheric effects, have been identified, and Hasan & Burrows (1995) summarize the corresponding theories for application to modelling of the HST PSF. These include the diffraction by pupil obscurations, geometrical aberrations, *microroughness of the main mirror and dust deposited upon its surface*. The last two phenomena produce extended wings, the effect being larger for the dust deposit, that dominates at large angles. The corresponding light is quite blue: the asymptotic wings are proportional to $\lambda^{-1.5}$ for the microroughness and to λ^{-2} for the dust. The OHP 120 telescope is probably rougher and dustier than the HST, and the amount of dust certainly increases with time, especially in summer. We thus have a qualitative explanation of the findings of Sect. 2.2.

There are possibly a number of photometric problems where the PSF far wings, *and specifically their changes with colour and mirror conditions*, might significantly affect the results. We suggest consideration of this eventual source of errors in specific cases, especially if dealing with extended and complex objects.

Acknowledgements. We thank our co-workers Dr. T. Idiart and J. de Freitas Pacheco for permission to use their observations in the present study. We are also indebted to the OHP staff, especially to the night assistants at the 120 cm telescope.

References

Bender, R., & Möllenhof, C. 1987, A&A, 177, 71

Capaccioli, M., & de Vaucouleurs, G. 1983, ApJS, 52, 465 (CdV83)

Carter, D. 1978, MNRAS, 182, 797

de Vaucouleurs, G. 1948, Ann. Astrophys., 11, 247

Hasan, H., & Burrows, C. J. 1995, PASP, 107, 289

Franx, M., Illingworth, G., & Heckman, T. 1989, AJ, 98, 538

Goudfrooij, P., Hansen, L., Jorgensen, H. E., et al. 1994, A&AS, 104, 179

Idiart, T., Michard, R., & de Freitas Pacheco, J. 2002, A&A, 383, 30

King, I. R. 1979, PASP, 83, 199

Lesser, M., & Venkatranan, I. 1998, in Proc. SPIE 3355, 608, ed. S. d'Odorico, Optical Astronomical Instrumentation

Michard, R. 1953, Ann. Astrophys., 16, 217

Michard, R. 1998, A&AS, 127, 299

Michard, R. 2000, A&A, 360, 85

Michard, R., & Marchal, J. 1994, A&AS, 105, 481

Mo, J., & Hanisch, R. J. 1993, in The Restoration of HST Images and Spectra, Space Telescope Sci. Inst. 1994, ed. R. J. Hanish, & R. L. White

Peletier, R. F., Davies, R. L., Illingworth, G. D., et al. 1990, AJ, 100, 1091

Sandage, A., & Tammann, G. 1981, Revised Shapley-Ames Catalogue of Bright Galaxies (Carnegie Inst. of Washington)

Schweizer, F. 1979, ApJ, 233, 23

Schweizer, F. 1981, AJ, 86, 662

Scorza, C., & Bender, R. 1995, A&A, 293, 20

Sirianni, M., Clampin, M., & Hartig, G. F. 1998, in Proc. SPIE 3355, 608, ed. S. d'Odorico, Optical Astronomical Instrumentation